2020 IEEE/RSJ International Conference on Intelligent Robots and Systems (IROS)
October 25-29, 2020, Las Vegas, NV, USA (Virtual)

Long-Reach Compact Robotic Arm with LMPA Joints for Monitoring of Reactor Interior

Akira Seino[1], Noriaki Seto[1], Luis Canete[2], and Takayuki Takahashi[1]

Abstract— **To reduce the risk of radiation leakages similar to the incident at the Fukushima Daiichi Nuclear Power Station, robots have been employed to remove fuel debris from reactors. To perform this process safely, it is important to monitor the interior of a reactor. A camera and neutron sensors are attached to the end of a robotic arm to monitor the interior of the reactor. The basic design requirement for the monitoring system is that the arm must be highly extendable and rigid. To achieve this, a novel compact long-reach manipulator with a joint structure built using a low-melting-point alloy (LMPA) is proposed. The LMPA enables switching between the free and locked states of the rotational joints of the manipulator. Herein, we first explain the design of the proposed joint structure and verify whether it has adequate mechanical strength. The required maximum torque to be sustained by the structure was calculated using the cantilever model, and the actual breaking torque was measured by the tensile test. Experimental results confirmed that the joint could withstand approximately 1.86 times the required torque. Finally, the effectiveness of induction heating, which is used to switch between the free and locked states of the joints, was evaluated experimentally. The LMPA arm was installed in the coil of the induction heating module, and the time required to melt LMPA was measured. The experimental results confirmed that the induction heating can change the state of the LMPA joint, and the time required for the melting is approximately 30.3 s. Therefore, the findings of this study show that the proposed system is capable of averting nuclear disasters through the prevention of radiation leakages at nuclear plants.**

I. INTRODUCTION

In 2011, a severe nuclear accident occurred at the Fukushima Daiichi nuclear power station, causing extensive damage and widespread contamination of the surrounding environment due to radioactive materials being discharged from the nuclear power station (NPS). To reduce the risk of radiation leakage incidents similar to the one at the Fukushima Daiichi Nuclear Power Station (F1NPS), it is recommended to remove fuel debris deposited inside the reactor. In Japan, this process is performed using robots. For investigating the inside of at the F1NPS, several robots were developed and deployed inside the reactor[1]–[7]. Nagatani et al. redesigned the mobile robot "Quince" to explore the interior and exterior of the reactor buildings[1][2]. Ohno et al. developed a robotic control vehicle equipped with the 3-D LIDAR, γ-cam, and a mobile robot "TALON" to measure radiation[3]. Kon et al. developed a mobile robot platform to monitor the outdoor environment and conducted out an experiment using the developed platform in a nuclear power plant[4]. Endo et al. developed a 10-m-long-coupled tendon-driven articulated manipulator, called the "Super Dragon," to investigate interior of the primary container vessel of the F1NPS[5]. Toshiba Corp. and International Research Institute for Nuclear Decommissioning (IRID) developed a small submersible crawling robot to investigate the pedestal interior of the reactor filled with water[6]. Mitsubishi Heavy Industries (MHI) and IRID developed a robotic arm to remove fuel debris from the F1NPS[7].

Safe and reliable methods should be employed to remove fuel debris from the reactor since it is highly radioactive. For removing debris safely, it is important to monitor the interior of the reactor to locate of the debris and obstacles. Cameras and neutron sensors have been used for monitoring the internal environment of reactors. The neutron sensor is required to approach the debris specifically when the radiation from the debris has to be measured. On the other hand, there is a limitation on size of the robot to be inserted owing to the dimension of the entrance opening on the pedestal.

A monitoring platform installed in the pedestal area that ensures simple and efficient monitoring of such an internal environment is proposed. The monitoring platform comprises of a monitoring arm, guide rail with mobile robots, remote control system, and an internal environment simulator. In this study, we propose a novel compact long-reach arm system for monitoring the interior of a reactor. The arm is composed of many short links connected serially via a joint and is capable of winding around a thin drum. A unique joint mechanism based on low melting point alloy (LMPA) to change its free and locked states is proposed in this study. This research focuses on conducting a basic study on two aspects: a LMPA joint structure and a heating device for switching the joint state.

The remainder of this paper is organized as follows. Section II describes the concept and overall image of the proposed arm.. In section III, we evaluate the prototype of the proposed arm and show that it has sufficient mechanical strength and is thus suitable for the practical applications. Section IV explains an experiment to confirm that induction heating could change the state of the LMPA joint. Finally, section V presents our conclusions.

[1]A. Seino, N. Seto and T. Takahashi are with the Faculty of Symbiotic Systems, Fukushima University, 1 Kanayagawa, Fukushima, Fukushima, 960-1296, Japan, {seino, taka}@sss.fukushima-u.ac.jp, seto@rb.sss.fukushima-u.ac.jp

[2]L. Canete is with the Department of Computer Engineering, University of San Carlos, Gov. M. Cuenco Ave, Cebu City, 6000 Cebu, Philippines, lscanete@usc.edu.ph

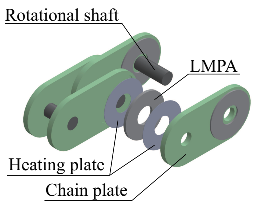

Fig. 1: Proposed structure of lock mechanism with LMPA.

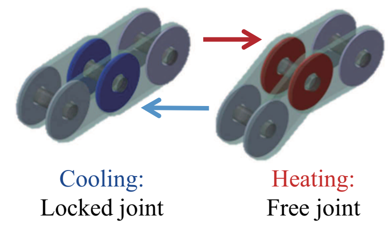

Fig. 2: The two states of the joint. The LMPA joint will be in a locked state when it is cooled and in a free state when it is heated.

II. ROBOTIC ARM DESIGN

A. Required specification

The target manipulator chosen for this study should satisfy the following three conditions:

1) The manipulator must have a high radiation resistance.
2) The end-effector must be capable of covering a wide are within the workspace.
3) The overall arm size must be smaller than the entrance on the pedestal.

The environment inside the pedestal has a high radiation dose due to fuel debris. The physical properties of some materials such as embrittlement and swelling (volume expansion) deteriorate due to the effects of radiation. Therefore, for long-term monitoring, the arm should have high radiation resistance.

According to the press releases of the Tokyo Electric Power Company (TEPCO), the diameter of the pedestal is approximately 5 m, and the distance between the monitoring platform and the bottom of the pedestal is approximately 3 m. The minimum required length of the arm was set as 3 m to perform sensing in this range.

In our study, an access hole (X-6 penetration) was used for the robot's entry into the pedestal. The diameter of the access hole was 547.6 mm. Therefore, the size of the robot has to be smaller than the diameter of the access hole. In addition, the target arm must be sufficiently small to enter the pedestal and sufficiently long to detect the debris inside the pedestal.

B. Investigation of existing robotic arm mechanisms

To begin with, we investigated existing compact long-reach arm mechanisms described in the previous studies, and compared them with the proposed novel mechanism. The telescopic mechanism described in[8] changes its length by feeding and storing the overlapping cylinders, while the boom mechanism described in[9] changes its length by sliding a multi-tiered bar-structure (boom) using a wire. The pantograph mechanism[10][11] can expand and contract by combining the multiple four-bar links and deforming them. The reel mechanism[12] changes its length by feeding and storing the convex similar to a tape measure. The chain mechanism[13]–[15] connects short links with hinges and expands and contracts by winding and unwinding the links.

The target arm must possess sufficient mechanical strength and rigidity to investigate a wide area. The end-effector will not be able to reach the target position due to bending of the arm if the strength and rigidity of the arm are low. Additionally, the arm sustains damage when it comes into contact with obstacles inside the reactor. The telescopic and boom mechanisms have a lower elongation ratio than other mechanisms. Increasing the strength and rigidity in these mechanisms results in an increase in their weight. The pantograph mechanism has high mechanical strength and a high elongation ratio; however, the backlash of each link connection is accumulated near the end-effector. As a result, a large deflection occurs in the end-effector. The reel mechanism has a high elongation ratio, and its size also decreases considerably when the arm is stowed. However the strength and rigidity are reduced in the extended state depending on the cross-sectional shape of the arm. The chain mechanism is similar to the rell mechanism in that it too has a high elongation ratio, and when the arm is stowed. However, when the arm is extended, the mechanical strength depends on the structure of the mechanism that connects the chains. Based on these investigation, the chain mechanism with a high elongation ratio was selected for this study. Additionally, we considered a hinge structure, which provides high strength and rigidity.

C. Hinge structure of the chain mechanism

The hinge structure influences the strength and rigidity of the chain mechanism. To satisfy these requirements described in sectionIIA, LMPA joint is proposed. Fig. 1 shows the image of a LMPA joint. A robotic arm is constructed by connecting multiple LMPA joints.

The LMPA joint locks the rotational motion by the shear strength of the LMPA. For unlocking the LMPA joint, the phase-change ability of LMPA is used. When the LMPA joint is heated, the LMPA melts, and the shear strength of the joint decreased. The concept of the locked/free mechanism of a LMPA joint is illustrated in Fig. 2.

The LMPA joint has two advantages. The first is its high energy effectiveness. At normal temperature, the LMPA is solid; thus, the joint is locked under normal conditions. In other words, the joint has to be heated only when it rotates. Therefore, there is no need to apply energy continuously in the normal state. The second advantage is its high rigidity. As the LMPA in the solid state is used to fix the rotation of the joint, the joint has no backlash. In addition, the joint can position the end-effector accurately.

D. Heating method

The LMPA joint changes its state of the joint using the phase change of the LMPA. We first compared the various heating methods that could be applied in the proposed system.

Joule heating is the simplest heating method. In this method, electrodes are connected to the heating material, and heat is generated due to the electrical resistance of the heating material. The advantage of this method is that the principle of

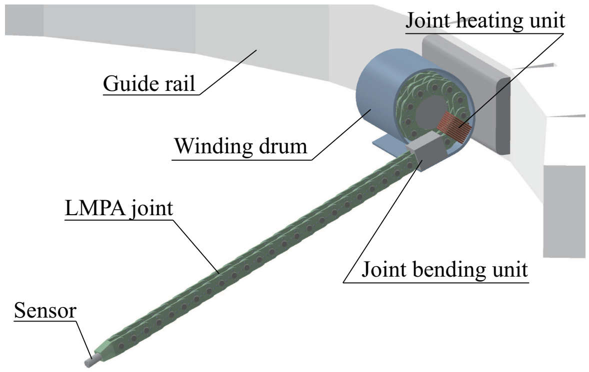

Fig. 3: Overview of the proposed arm system with LMPA joints for monitoring the pedestal.

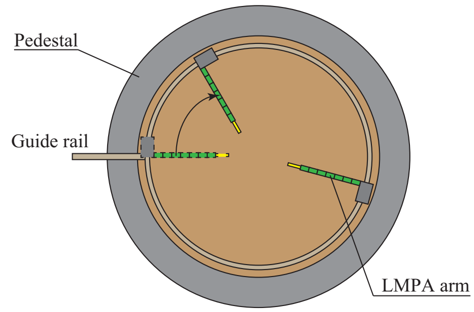

(a) Top view

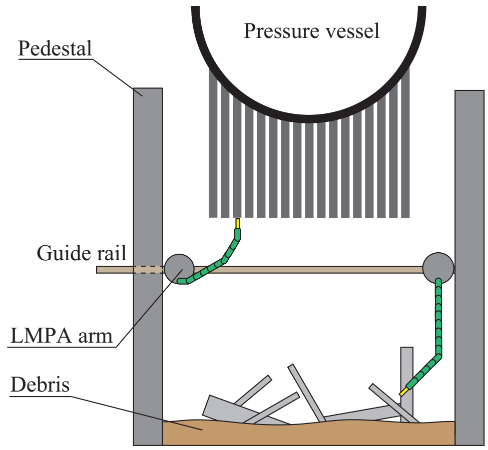

(b) Side view

Fig. 4: The image of the debris monitoring in the pedestal captured by the proposed LMPA arm.

the heating mechanism is simple, and the heating control can be achieved effortlessly. However, the mechanical structure of the heating device and the LMPA joint becomes complex because the electrodes have to be connected to the heating material.

Dielectric heating is a non-contact heating method. This method uses a high-frequency electric field for heating a dielectric material such as rubber or resin. The advantage of dielectric heating is that it is capable of providing uniform heating in a short time. However, this method is not sage because, when a metal is heated using the dielectric heating method, it gets electrified and causes sparks.

Induction heating (IH) is widely known as a non-contact type heating method. This method uses a high frequency alternating magnetic field for heating a conductor. This method is suitable for our study because heat is induced in the object itself. Moreover, it is possible to achieve high-temperature heating rapidly because the energy per unit time supplied to the object to be heated by the coil is high. However, the heating efficiency depends on the heated material and the shape of a coil.

The proposed manipulator is assumed to be used in the F1NPS. Currently, the pedestal in the F1NPS is injected with cooling water. Hence, the manipulator is drenched in water during the monitoring process. For these reasons, the heating method must be non-contact type, and the heating equipment must be simple. Finally, the induction heating method was selected for this study to invoke phase change in LMPA.

E. Overview of the proposed manipulator system

Based on the discussion thus far, an overview of the proposed system is shown in Fig. 3. The proposed monitoring arm system consists of an arm structured using multiple LMPA connected joints, an IH unit, sensors at the end-effector, an arm winding device, a joint angle changing unit, and a guide rail.

The robotic arm is supposed to approach the top of the debris settled at the bottom of the pedestal. Fig. 4 illustrates the monitoring operation performed using the proposed system. The arm is compactly wound around the drum when the robotic arm enters inside the pedestal. The robotic arm is mounted on the mobile robot, and the mobile robot runs along the guide rail. After the robot enter inside the pedestal, the LMPA joints in the work coil are heated successively to release the locked state in order to extend the arm towards the object, and the winding drum is rotated to extend the joint. At this instant, the joint bending unit sets the LMPA joint, which is in the free state, to an arbitrary angle. When the bent joint cools down, it can retain the angle. As this operation must be repeated, the sensor can be brought to the orbital position from above the debris, and obstacle avoidance can be achieved conveniently under certain conditions. A neutron sensor mounted on the end-effector measures the radiation dose of the debris. When the arm is shortened, the heating unit changes the locked state of the LMPA joint to the free state, and the winding drum rotates and winds up the arm.

When the arm is extended, elastic deformation may occur due to the weight of the arm and the sensors such as a camera mounted on the end-effector. Hence, position control must be applied to the robotic arm using the sensor of the end-effector.

III. LMPA JOINT

A. Structure of the LMPA joint

As mentioned above, the LMPA arm is constructed using multiple LMPA joints. Fig. 5 shows the mechanical structure

TABLE I: List of materials used in the LMPA joint

Parts	Materials
LMPA	Solder (Sn:Pb = 60:40)
Chain plate	Glass epoxy
Heating plate	Tinplate
Countersunk rivet	Steel
Rotational shaft	Brass

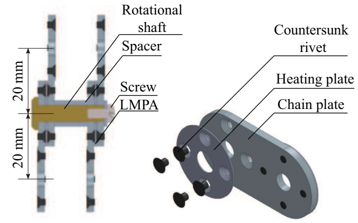

Fig. 5: The mechanical structure of a LMPA joint

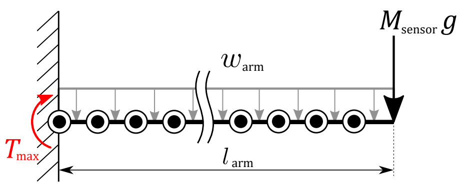

Fig. 6: The model of the maximum torque generated at the base of the LMPA arm

of a single LMPA joint. The two chain plates with a heating plate are placed facing each other with a small gap between them. This gap is filled with LMPA. The chain plate and the heating plate are mechanically fixed using countersunk rivets. When a large external force is applied on the joint, the solidified LMPA breaks. However, two chain plates can be reconnected by reheating. Finally, taking torsion into account, two sets of LMPA joints are arranged in parallel with a distance.

The material of each component of the LMPA joint is listed in Table I. Cooling water is injected into the pedestal of the F1NPS, and the internal temperature is observed to be lower than 100 °C. A LMPA is selected as the solder due to its availability and melting temperature. The melting point of the solder is 183 °C. Therefore, the solder is solidified in the pedestal of the F1NPS without heating. Glass epoxy is used to fabricate the chain plate because of its high radiation resistance (30 MGy) and low thermal conductivity (0.29–0.42 W/mK). Due to its high saturation magnetic flux density, tinplate is selected for fabricating the heating plate. Steel is used as the material of the countersunk rivet because of two reasons. First, steel rivets generate heat due to their high magnetic permeability, and thus, heating can be achieved quickly. Second, steel can produce intermetallic compounds with contained in LMPA (solder), and thus, the bonding surface of the solder can be expanded.

B. Strength test

An experiment is conducted to confirm whether the designed prototype has adequate mechanical strength.

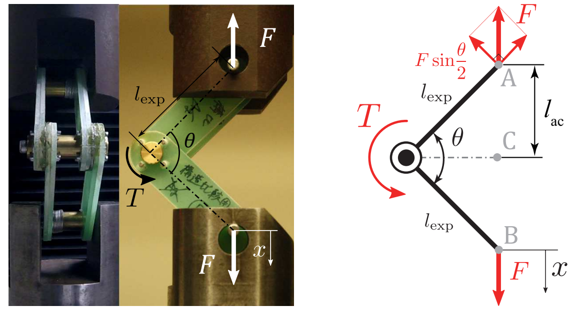

(a) Experimental setup (b) Analyzing model

Fig. 7: Tensile test for evaluating the breaking strength of single LMPA joint. The upper fixture does not move, and the lower fixture translates downward in the image.

1) Modeling the maximum load on the joint: The torque applied to the joint of the arm is calculated by considering the weight of the arm and the sensor attached to the end-point. When the arm extends linearly in the horizontal direction, the torque generated by the sensor will be maximum at the base joint of the arm. The arm to be modeled is assumed to be a cantilever that bears a uniform load along its length due to its own weight and the concentrated load of the sensor is applied to the end-point. The maximum torque T_{max} is calculated as:

$$T_{\text{max}} = \frac{1}{2} w_{\text{arm}} g l_{\text{arm}}^2 + M_{\text{sensor}} g l_{\text{arm}}, \tag{1}$$

where w_{arm} kg/m represents the mass per unit length of the arm, M_{sensor} kg represents the mass of the sensor, and l_{arm} m represents the length of the arm.

In our study, the values used for these parameters are $w_{\text{arm}} = 0.764$ kg/m, $M_{\text{sensor}} = 1.0$ kg, and $l_{\text{arm}} = 3.0$ m. Upon substituting these values, the maximum torque T_{max} was calculated to be approximately 63.2 Nm. Hence, the breaking torque of the joint must be higher than 63.2 Nm.

2) Measurement of the breaking torque: The tensile test was conducted to measure the breaking torque of the joint. The experimental setup is shown in Fig. 7(a). The LMPA joint of the test piece and the two sets of LMPA joints arranged in parallel in the actual LMPA arm were used for the tensile test. To compare the effect of the chain plate deflection, a test piece with a fixed rotating shaft was also used. The initial joint angle of the test piece θ_0 was 90 °, and an universal testing machine was used to pull the both ends of the test piece with pulling force F N. The tensile tests were performed thrice.

From Fig. 7(b), we calculate the torque T using the pulling force F. In this model, the points A and B are attached to the fixed part, and moving part of the universal testing machine, respectively. We define T_{upper} and T_{lower} as the torques generated around shaft by the upper link and the lower link, respectively. Then, T_{upper} is calculated as

$$T_{\text{upper}} = l_{\text{exp}} F \sin\left(\frac{\theta}{2}\right), \tag{2}$$

TABLE II: Measured breaking torque of the LMPA joint

Test number	Breaking torque Nm
1	120.1
2	126.5
3	106.4
Average	117.7
S.D.	10.27

where l_{exp} represents the length of the upper link, and θ represents the angle between the two links. When the lengths of the upper link and lower link are equal, the torque T around the rotational joint is the sum of the torques T_{upper} and T_{lower}. Next, the relationship between the angle θ and the displacement x of point B must be considered. Let l_{AC} be the length between the points A and C; then, l_{AC} is calculated as

$$l_{\text{AC}} = l_{\text{exp}} \sin\left(\frac{\theta_0}{2}\right) + \frac{x}{2}, \tag{3}$$

where x is the movement distance of the universal test machine fixture. From the geometric relationship between points A, C, and the joint,

$$\sin\left(\frac{\theta}{2}\right) = \frac{l_{\text{AC}}}{l_{\text{exp}}}, \tag{4}$$

$$\theta = 2\sin^{-1}\left\{\sin\left(\frac{\theta_0}{2}\right)\right\} + \frac{x}{2l_{\text{exp}}}. \tag{5}$$

Based on (5), the joint angle θ is calculated using the displacement x.

3) Results and Discussion: The relationships between the angle θ and the measured torque T for all trials are shown in Fig. 8. The breaking torque values measured during all three tensile tests are listed in Table II. Fig. 8 confirms that the inclination of the test piece with the fixed joint is nearly the same as that of the normal test piece in the initial state, below 95 °. Therefore, the initial deflection is mainly caused by the deformation of the glass epoxy chain plate.

The safety ratio S to meet the evaluation criteria is defined as

$$S = \frac{\sigma_{\text{c}}}{\sigma_{\text{a}}}, \tag{6}$$

where σ_{c} represents the representative strength and σ_{a} represents the allowable strength. In this experiment, σ_{c} was 117.7 Nm, and σ_{a} was 63.2 Nm. Hence, S was found to be 1.86. In other words, these results confirmed that the proposed LMPA joint had sufficient strength, and therefore, could be used in the arm of the proposed monitoring system.

IV. HEATING EXPERIMENT

A heating experiment conducted to verify the heating performance of IH is explained in this section.

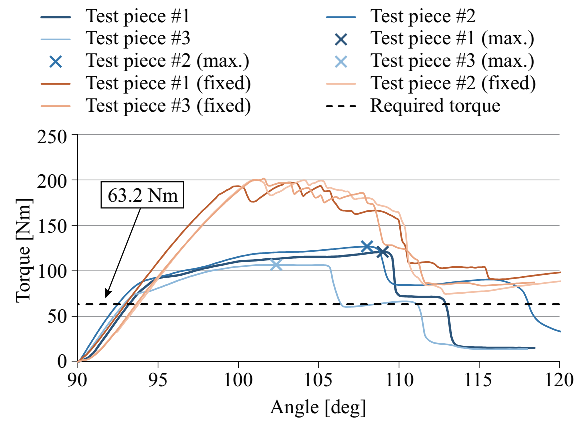

Fig. 8: The relationship between the angle θ and measured torque T around the joint is illustrated. Blue lines represent the experimental results of the test pieces. Orange lines represent the experimental results of the test pieces with the fixed rotational joint. Black dotted line represents the required maximum torque T_{max} (63.2 Nm). Cross marks represent the maximum torque (breaking torque) of each test piece.

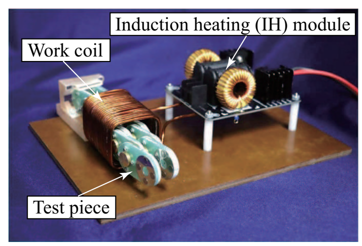

Fig. 9: An experimental setup to measure the heating speed of the LMPA arm.

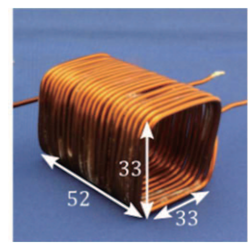

Fig. 10: The size of the coil used in the experiment.

A. Experimental method

Fig. 9 shows the experimental setup. The LMPA arm, which was selected as the test piece, was inserted inside a work coil after being lifted off the ground using a jig. The coil had a width 45mm, height of 40mm, and length of 36mm (number of coil turns: 16), as illustrated in Fig. 10. The voltage applied to the IH module is set to 20, 25, and 30 V. In this experiment, we measured the time before the LMPA in the joint melted. The duration between the start of heating (Fig. 11(a)) and the time at which the arm began to bend and approach the ground (Fig. 11(b)) is the time required for melting.

B. Results and discussion

The measurement are listed in Table III. The experiments confirmed that induction heating changes the free and locked states of the LMPA joint. When the applied voltage was 20 V, the time taken to melt the LMPA was 95.8 s. As the applied voltage increases, the time required for melting also decreases. When the applied voltage was 30 V, the time required for melting was found to be 30.3 s.

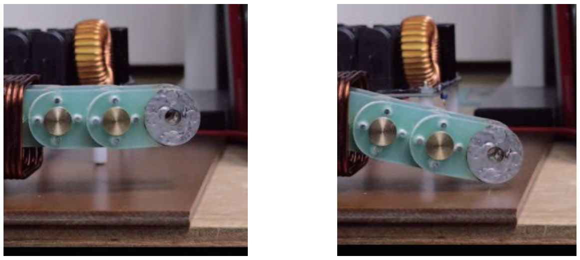

(a) Before melting (b) After melting

Fig. 11: Heating experiment conducted on the LMPA arm.

TABLE III: Time required to melt the LMPA arm

Applied voltage V	Time s
20	95.8
25	48.1
30	30.3

However, the speed at which melting is achieved is not sufficient in practical applications. There are two main reasons for the substantial heating time in this experiment. First, the work coil encloses multiple LMPA joints. In this experiment, the LMPA joints could not be heated successively due to the size of the coil. Therefore, the speed at which each joint was heated decreased because multiple joints were being heated simultaneously. To solve this problem, the structure of the coil including the size and shape of the cross-section, must be improved. The second reason is assumed to be the influence of other components on the heating material. Countersunk rivets and rotating shafts, which are components of the LMPA joint, are also heated in addition to the heating material while the joint is heated. In other words, when more materials are heated simultaneously, the time taken for heating increases. In addition, it is assumed that the effect of heat dissipation from each material is also involved; therefore, further investigation is needed to determine which materials affect the heating.

V. CONCLUSION

In this study, we proposed a novel compact long-reach manipulator mechanism. The proposed manipulator is constructed by connecting LMPA joints in the form of a chain. The free and locked states of a LMPA joint can be changed by invoking phase change of LMPA.

To confirm the suitability of the LMPA joint for its application in the pedestal monitoring robotic arm, the strength of the joint was verified through a tensile test. The required maximum torque calculated using the cantilever model was found to be 63.2 Nm, and the measured breaking torque was 117.7 Nm. The results confirmed that the proposed joint structure possessed adequate mechanical strength.

The time required to melt the LMPA arm was measured through an experiment, to evaluate the effectiveness of induction heating in melting the LMPA. From the experiment, it was confirmed that induction heating could be used to change state of the LMPA joint. The experiment was performed using an applied voltage of 30 V, and the time required to melt the LMPA was found to be approximately 30.3 s. The findings of this study show that the developed manipulator configuration is suitable for monitoring reactors. Therefore, the proposed system has the potential to avert nuclear disasters through the prevention of radiation leakages at nuclear plants.

For future applications, the heating equipment must be improved and optimized to increase the heating rate. In a subsequent study, we plan to integrate the LMPA arm and induction heating unit to construct the arm system.

REFERENCES

[1] K. Nagatani, S. Kiribayashi, Y. Okada, S. Tadokoro, T. Nishimura, T. Yoshida, E. Koyanagi, and Y. Hada, "Redesign of rescue mobile robot Quince," 2011 IEEE International Symposium on Safety, Security, and Rescue Robotics, Kyoto, 2011, pp. 13-18.

[2] K. Nagatani, S. Kiribayashi, Y. Okada, K. Yoshida, S. Tadokoro, T. Nishimura, T. Yoshida, E. Koyanagi, M. Fukushima, and S. Kawatsuma, "Emergency response to the nuclear accident at the Fukushima Daiichi Nuclear Power Plants using mobile rescue robots", Journal of Field Robotics, Vol. 30, No. 1, 2013, pp.44-63.

[3] K. Ohno, S. Kawatsuma, T. Okada, E. Takeuchi, K. Higashi and S. Tadokoro, "Robotic control vehicle for measuring radiation in Fukushima Daiichi Nuclear Power Plant," 2011 IEEE International Symposium on Safety, Security, and Rescue Robotics, Kyoto, 2011, pp. 38-43.

[4] K. Kon, H. Igarashi, F. Matsuno, N. Sato and T. Kamegawa, "Development of a practical mobile robot platform for NBC disasters and its field test," 2012 IEEE International Symposium on Safety, Security, and Rescue Robotics (SSRR), College Station, TX, 2012, pp. 1-6.

[5] G. Endo, A. Horigome, and A. Takata, "Super Dragon: A 10-m-long-coupled tendon-driven articulated manipulator," IEEE Robotics and Automation Letters, vol. 4, no. 2, April, 2019, pp. 934-941.

[6] Toshiba Corp. [Online], https://www.toshiba.co.jp/about/press/2017_06/pr1501.htm (Accessed 6 February 2020)

[7] Japan Atomic Industrial Forum, Inc. [Online], https://www.jaif.or.jp/en/demonstration-made-by-mhi-and-irid-of-robot-arm/ (Accessed 6 February 2020)

[8] T. Fujioka, G. Endo, K. Suzumori, and H. Nabae, "Proposal of tendon-driven elastic telescopic arm and initial bending experiment," 2017 IEEE/SICE International Symposium on System Integration (SII), Taipei, 2017, pp. 164-169.

[9] T. Hashimoto, T. Tomizawa, A. Ohya and S. Yuta: "Development of a general-purpose expandable arm for small mobile robots", Proceedings of the Third International Conference on Autonomous Robots and Agents, pp. 397-401.

[10] A. Shikari and H. Asada, "Triple scissor extender robot arm: a solution to the last one foot problem of manipulation," in IEEE Robotics and Automation Letters, vol. 3, no. 4, 2018, pp. 3975-3982.

[11] S. Teshigawara and H. Asada, "A mobile extendable robot arm: singularity analysis and design*", 2019 IEEE/RSJ International Conference on Intelligent Robots and Systems (IROS) Macau, China, 2019, pp.5131 - 5138.

[12] K. Tanaka, H. Yokoyama, H. Ishii, S. Inoue, Q. Shi, S. Okabayashi, Y. Sugahara, and A. Takanishi, "Novel extendable arm structure using convex tapes for improving strength of pipe on tiny mobile robots," 2016 IEEE International Conference on Robotics and Biomimetics (ROBIO), Qingdao, 2016, pp. 637-642.

[13] Tsubakimoto Chain Co., [Online], https://tsubakimoto.com/power-transmission/linear-actuator/zip-chain-actuator/zca/?_ga=2.126256269.1444694300.1580977305-504507253.1580977305 (Accessed 6 February 2020)

[14] Life Robotics Inc. [Online], https://liferobotics.com/product/ (Accessed 6 February 2020)

[15] F. Collins and M. Yim, "Design of a spherical robot arm with the Spiral Zipper prismatic joint," 2016 IEEE International Conference on Robotics and Automation (ICRA), Stockholm, 2016, pp. 2137-2143.